JMEPEG (2016) 25:1407–1415
DOI: 10.1007/s11665-016-1969-8

1059-9495/$19.00

Friction and Wear Behavior of 30CrMnSiA Steel at Elevated Temperatures

Sheng-guan Qu, Fu-qiang Lai, Guang-hong Wang, Zhi-min Yuan, Xiao-qiang Li, and Hui Guo

(Submitted September 30, 2015; in revised form January 19, 2016; published online February 22, 2016)

The friction and wear properties of 30CrMnSiA steel were investigated at elevated temperature from 100 to 600 °C. Thereafter, the wear debris and worn surfaces were examined to understand the wear mechanisms. The remained debris with relatively high hardness created three-body abrasion at lower temperatures (100-300 °C). Abrasive wear prevailed at the conditions with high friction coefficients and wear rates. A significant change in friction and wear behavior occurred at 400 °C. At the temperature of 400 °C, oxidation induced mild wear was found because of the formation of load-bearing oxide film. Both the friction coefficients and wear rates of the steel were lowest at 400 °C. At the temperatures of 500-600 °C, a mild-to-severe wear transition occurred which resulted in an increase in the friction coefficients and wear rates of the steel. This is related to the decrease in the strength of matrix and hardness of worn surfaces and subsurfaces. The predominant wear mechanism is considered to be severe abrasive, adhesive wear and a fatigue delamination of the oxide film.

Keywords friction coefficient, oxidative wear, steel, wear mechanism

1. Introduction

30CrMnSiA steel is typically used as mechanical parts in equipment manufacturing and aerospace industries, because of its excellent mechanical properties such as high strength and toughness after quenching and tempering (Ref 1-5). High-temperature mechanical properties, constitutive relationships and micro-damage behaviors of 30CrMnSiA steel have been reported in Ref (1, 2). Moreover, laser quenching of plasma nitrided 30CrMnSiA steel and the effects of rare earths addition on microstructure and wear resistances were investigated (Ref 3-5). It has been mentioned that most of the parts serve at elevated temperatures and slide against each other at low speeds in dry condition (Ref 6). Service temperature considerably influences on the extent of wear damage of metallic components (Ref 7, 8). Numerous studies were performed on high-temperature wear of various steels where new understanding and advanced major concepts of tribology were discussed (Ref 9-15). However, the friction and wear behavior of 30CrMnSiA steel after quenching and tempering at high temperature are seldom reported. Based on the application of 30CrMnSiA steel, it is necessary to study the effect of temperature on the wear resistance of 30CrMnSiA steel.

In this study, wear tests of 30CrMnSiA steel at elevated temperatures were performed. The dependency of the ambient temperature on friction and wear behavior was explored, and the high-temperature mechanisms were discussed.

Sheng-guan Qu, Fu-qiang Lai, Guang-hong Wang, Zhi-min Yuan, and **Xiao-qiang Li**, School of Mechanical and Automotive Engineering, South China University of Technology, Guangzhou 510640 Guangdong, China; and **Hui Guo**, Department of Materials Physics and Chemistry, University of Science and Technology Beijing, Beijing 100083, China. Contact e-mail: lfq0623@163.com.

2. Materials and Experimental Procedure

The friction and wear tests were accomplished using a high-temperature wear tester (MMU-10G type); the schematic of the test chamber is shown in Fig. 1. The upper rotating specimen is made of hardened AISI 52100 steel with high hardness (60 HRC) (Ref 15), and the cylinder is counterpart with inner radius of 10 mm and outer radius of 12.8 mm. The surface roughness, R_a is found to be less than 1.2 μm. The lower stationary specimen is a disk of φ43 mm × 4mm made of 30CrMnSiA steel. The chemical compositions of the two types of steels are shown in Table 1. The 30CrMnSiA steel was austenitized at 890 °C for 0.5 h and quenched in oil. Tempering was accomplished at 540 °C for 3 h, followed by air cooling to reach room temperature. Table 2 shows the mechanical properties of the 30CrMnSiA steel.

The tests were carried out at a temperature range from 100 to 600 °C without lubrication. The other parameters were set as follows: normal applied pressure of 1.5 MPa, running time of 4200 s, and sliding speed of 0.036 m/s for first 600 s during running-in process and 0.072 m/s in the remaining time. During the tests, the friction coefficient was automatically recorded. Before and after wear tests, the specimens were cleaned in a solution containing of petroleum ether and alcohol in ultrasonic cleaner for 20 min. The wear weight losses of the specimens were obtained using an electronic balance with an accuracy of 0.1 mg. The profiles of the disk worn surfaces were characterized using a BMT profile device which is helpful to understand the wear mechanism. The wear rate was calculated using the following equation:

$$W = V/(P \cdot L) = \Delta m/(\rho \cdot P \cdot L), \quad \text{(Eq 1)}$$

where W is the wear rate, Δm represents the wear weight loss, ρ is the density of specimens, P is the normal applied load,

Table 1 Compositions of the two steels (wt.%)

Steel	C	Cr	Mn	Si	P	S	Fe
30CrMnSiA	0.25-0.35	0.9-1.1	0.9-1.1	0.9-1.1	<0.01	<0.01	Bal.
AISI 52100	0.95-1.05	1.40-1.65	0.25-0.45	0.15-0.35	≤ 0.025	≤ 0.025	Bal.

Table 2 Mechanical properties of the 30CrMnSiA steel

Steel	σ_b at R.T.	σ_s at R.T.	σ_b at 600 °C	σ_s at 600 °C	Elongation at R.T.	Hardness at R.T.	Impact energy at 0 °C
30CrMnSiA	1008 MPa	914 MPa	375 MPa	330 MPa	15.1%	32.1 HRC	15.2 J

and L is the sliding distance (Ref 16). Data presented are the average of three experimental results. A scanning electron microscope (SEM) coupled with an energy-dispersive spectroscopy (EDS) were used to analyze the topographical features of the worn surfaces and the wear debris. An x-ray diffractometer (XRD, Cu Kα radiation) was used to identify the phase of the debris.

3. Results and Discussion

3.1 Friction Coefficients

Figure 2 shows the typical evolution of friction coefficients with respect to time at 100-600 °C with an interval of 100 °C. It is evident that the fluctuation of friction coefficient was violent during running-in stage at lower speed (0.036 m/s) for first 600 s. It seems that there may be a correlation between the ambient temperature and the wear behavior. At lower temperature, the friction coefficient reaches 0.8 after 900 s, whereas it becomes stable after 500 s at 200 °C. However, there is no distinct variation of friction coefficient at 400 °C. Moreover, friction coefficient takes hundreds of seconds to become steady state at high temperatures (500 and 600 °C) in the initial stage and then severely fluctuates in the subsequent stage. It is noted that the running-in stage becomes shorter with increasing temperature, which was also found in Ref (17).

Figure 3 displays the average friction coefficient in steady-state at different temperatures. The friction coefficient is highly related to the ambient temperature. From 100 to 400 °C, an increase of temperature results in a decrease in friction coefficient. The mean value of the friction coefficients is about 0.73 at 100 °C, and it decreases to 0.40 at 400 °C. However, the mean value of the friction coefficients gradually increases beyond 400 °C. It increases to 0.55 at 600 °C. It is worth mentioning that the lowest friction coefficient is obtained at 400 °C.

3.2 Wear Resistance

As the high-temperature oxidation influences the wear results, it is necessary to account for the oxidation in wear tests. Therefore, a stationary oxidation test was simultaneously performed. After the test, the specimens are weighed to quantify the oxidation. It is found that negligible oxidation occurs at low and medium temperature (100 to 400 °C), and the specimens gain a bit weight at high temperature (500, 600 °C). The value would be subtracted from the wear values obtained in the wear tests.

The wear rates of 30CrMnSiA steel at different temperatures are shown in Fig. 4. With increasing temperature from 100 to 300 °C, the wear rate firstly increased and then slightly decreased.

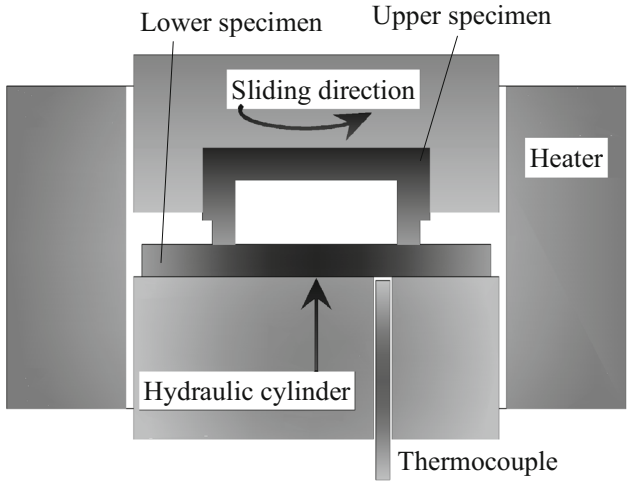

Fig. 1 Schematic of the high-temperature wear tester (MMU-10G) used

When the temperature reached 400 °C, the wear rate sharply declined, and it is related to the friction coefficients behavior as shown in Fig. 2 and 3. For many metals and alloys, there is apparently a transition temperature in wear behavior (Ref 8, 13, 18-20). The transition temperatures of friction and wear of M50 high-speed steel was 400 °C (Ref 13). Further, the critical temperature of 316 stainless was found to be above 300 °C (Ref 18). The increase in wear rate at 500-600 °C can be attributed to the decrease in hardness, surface, and oxide film damage occurred at high temperature. It can be inferred that the wear rate at high temperature is much lower than that at low temperature, which is closely associated with the difference in wear mechanisms. The obtained results are in good agreement with Ref (21).

3.3 Morphology and XRD Analysis of Wear Debris

The morphologies of the wear debris after testing at 200, 400, and 600 °C are shown in Fig. 5(a)-(c), respectively. During the tests, many particles were pushed out of the rubbing interfaces, while others remained in the interfaces. The remained debris were fractured, ground, rolled, oxidized, and compacted into layers due to the sliding action. Thus, most of the debris (oxide particles) is found to be very small in size (fine abrasive powder) at low and medium temperature. The decrease in hardness of the steel at high temperature made the surface and the compacted layers to be plowed more violently. As a result of the continuous micro-cutting or fatigue by repeated deformation (plowing) of the materials during the tests, more large fragments were generated at high temperature.

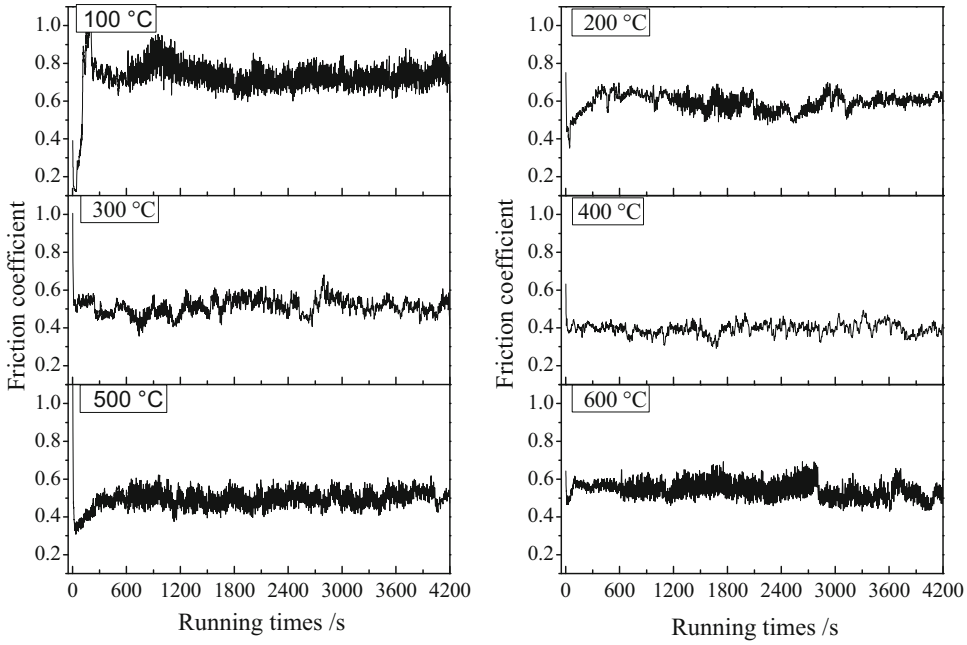

Fig. 2 Friction coefficients at the function of time at different temperatures

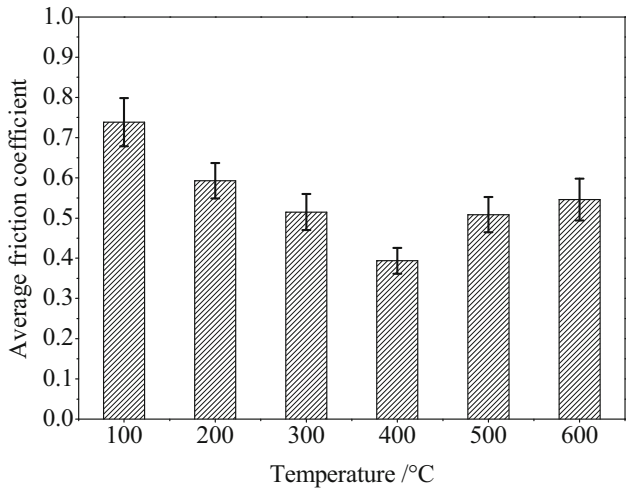

Fig. 3 Friction coefficients in steady state at different temperatures

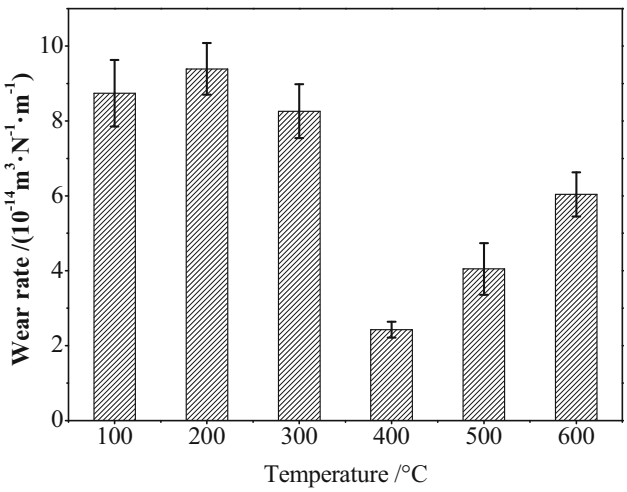

Fig. 4 Wear rates of 30CrMnSiA steel at different temperatures

Figure 5(d) shows the XRD patterns of the wear debris at different temperatures. Similar to Ref (21), only Fe and Fe_2O_3 were identified in the debris at different temperatures. However, some studies also identified Fe_3O_4 on worn surfaces of pin specimens (Ref 22, 23). Fe appeared in the debris at all temperatures and with lowest amount at 400 °C. The amount of Fe_2O_3 gradually increases with increasing temperature, associated with the higher temperature causing a more significant oxidation of debris (Ref 17).

3.4 Worn Surface Morphology and Wear Mechanism

The wear mechanisms of 30CrMnSiA steel at different temperatures were investigated after the tests. Thick white arrows indicate the sliding directions of upper specimens. It is believed that the wear debris particles were generated from the relative movement of contact surfaces. Thus, many of the debris would remove from the rubbing interface due to the sliding, leading to wear loss of specimens. Additionally, other debris particles were retained between the rubbing surfaces.

At a lower temperature (200 °C), retained debris between the contact surfaces assumed to be displayed high hardness compared to the disk surface, especially the debris generated from the harder specimen. These debris remained and agglomerated in the contact zone as moving particles plowing the surfaces to generate the grooves and abrasive pits as shown in Fig. 6(a) and (b). Thus, the system can be treated as three-body abrasion. If the hard debris would embed in one surface, the system may act as two-body abrasion to cause damage to the other surface (Ref 8). As the abrasion and sliding continues, the retained debris were ground, rolled, oxidized, and fractured. Hence, they became fine abrasive powder. The whole processes could be illustrated in Fig. 6(c) and (d). Some of the fine debris

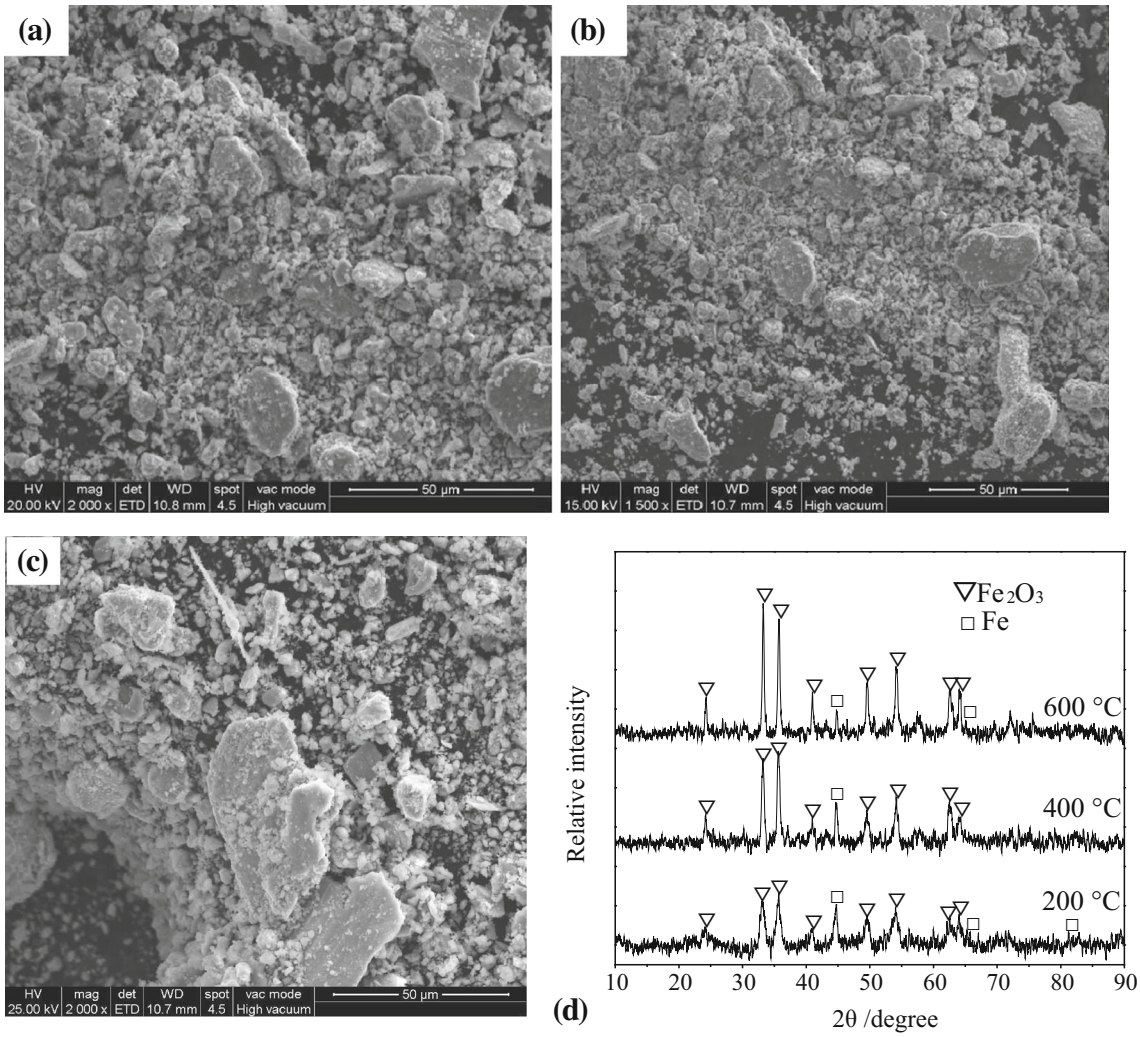

Fig. 5 SEM micrographs of the wear debris collected from the interface under sliding at (a) 200 °C, (b) 400 °C, and (c) 600 °C, and (d) XRD patterns of the wear debris

were compacted into oxide layers (Fig. 6b). Under the compaction and repeated abrasion and sliding, the oxide layers could be fractured as adhesive trace, exposing fresh areas of clean metal to the oxidative environment. With the removal of existing oxide layers, metal-metal contact may result in the formation of metallic debris (Ref 7). In summary, there are usually various wear mechanisms at the high-temperature dry sliding system. The dominant wear mechanism at low temperature is abrasive wear.

At 400 °C, the morphologies of the worn surfaces are much different with those at 200 °C. As shown in Fig. 7(a) and (b), a slightly rough oxide layer can be observed on the worn surfaces, covering the surfaces in a large scale. A smooth oxide layer can be also found on the worn surfaces (Fig. 7c). A 3D topography of worn surfaces is shown in Fig. 7(d); the cross-section profile of worn surfaces at 400 °C is shown in Fig. 8(f).

It has been reported by many authors (Ref 7, 8, 22, 24, 25) that protective oxide film is generated in many system surfaces at high temperature during sliding test. During the test at 400 °C, the debris retained between rubbing interfaces would experience other processes compared to those at lower temperature. In fact, the retained fine particles were compacted and sintered together to some extent to form more solid layers. The sintering of particles is more significant at higher temperature, and the consolidation of the layers is facilitated by the oxidational environment (Ref 8). As sliding continues, the spalling of the layers and the sintering between particles would occur competitively. It is mentioned that the spalling of the oxide is only a part of the whole thickness of the layer (Ref 22), and the mild separation is shown in Fig. 7(b). Under the scratching and burnishing, some of the layers may be formed as a "glaze" layer, as shown in Fig. 7(c). High temperature is helpful to the sintering and the oxidation of particles and induces Fe_2O_3 as shown in Fig. 5(d). If the sintering process dominates over spalling, the wear of rubbing surfaces decreases to a very low value due to the formation of the oxide layer. Consequently, the oxide film covered on the surfaces in a large proportion to prevent the direct contact of the 30CrMnSiA steel and its coupled part, giving an effective protection to the rubbing pairs. Hence, the oxide film became wear-protective load-bearing layers. This accounts for the conception of a critical temperature below which the wear rate is high and at which it is relatively lower (Ref 25).

Furthermore, mild wear traces were found in Fig. 7(g) and (h), which are the representative of the morphologies of worn surfaces of AISI 52100 steel. These are helpful to explain the change in friction coefficients and wear rates shown in Fig. 2

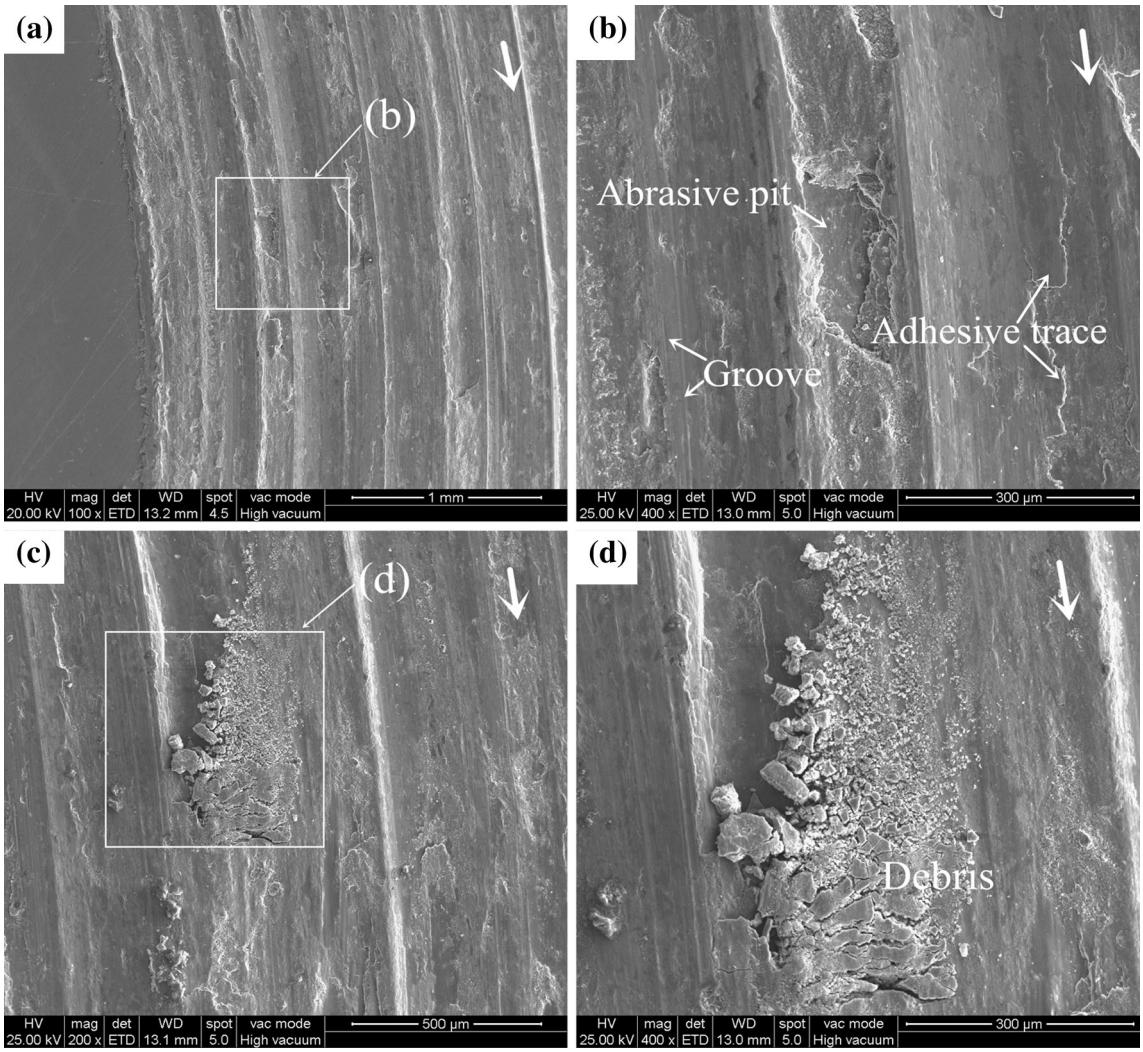

Fig. 6 Morphologies of worn surfaces of 30CrMnSiA steel at 200 °C

and 4 at 400 °C. The friction coefficient and wear rate at 400 °C were lowest.

Figure 7(e) and (f) show the morphology of the oxide film on the worn surface at 400 °C and EDS analysis of the black line marked in the figure. It can be observed that the oxide layers and some zones of surface are scratched, leaving a fresh surface of the body indicated by the blank ellipse (Fig. 7e). Some cracks appeared on the oxide layer related to the damage of the film. An abrupt change in both the content of iron and oxygen at the junctions between the matrix and the oxide film can be noticed (Fig. 7f). The oxygen content in oxide film is remarkably high, whereas it is rarely found in the matrix where the iron is a predominant element. It is clear that the covering layer is oxygen-rich compound. The minimal wear rate at 400 °C can be explained by the formation of oxide film on the worn surface and its separation under sliding (Ref 22). According to the mild oxidation wear mechanism, the separation rate of the oxide film and the rate of formation of oxide film will reach an equilibrium state, which can be termed as an 'oxidation-separation-reoxidation' mechanism. It is in good agreement with Ref (11, 22, 25). It can be concluded that a kind of oxidational wear prevails at medium temperature (400 °C), which is termed as the mild oxidative wear.

The characteristics of worn surfaces after wear test at 600 °C are shown in Fig. 8. As previously mentioned, the debris particles generated from the rubbing surfaces contain the removed debris and the retained debris. Figure 8(a) and (b) shows the agglomeration, compaction, and sintering of the retained debris during the early stages of sliding. Moreover, debris were found on the surfaces out of the rubbing border as they were not cleaned. Serious delaminated crater and abrasive traces can be found on worn surfaces (Fig. 8c and d). In addition, oxide film fractured near the crater.

It has been reported that the mechanical properties of the 30CrMnSiA steel would sharply decrease at high temperature (Ref 6). The tensile strength of 30CrMnSiA steel decreased from 1008 MPa at room temperature to 375 MPa at 600 °C (Table 2). The high temperature resulted in the severe decrease in the hardness in the steels (Ref 26), which leads to the softening of worn surface and subsurface. Abouei et al. (Ref 15) indicated that a harder matrix can hold the compact oxide film more firmly than a softer one. Consequently, it can be assumed that the matrix at 600 °C would be not strong enough to hold/support the oxide film. When the friction forces reach to the tensile strength of metal and the bonding strength between the oxide film and matrix, severe wear occurs (Ref 22). Hence,

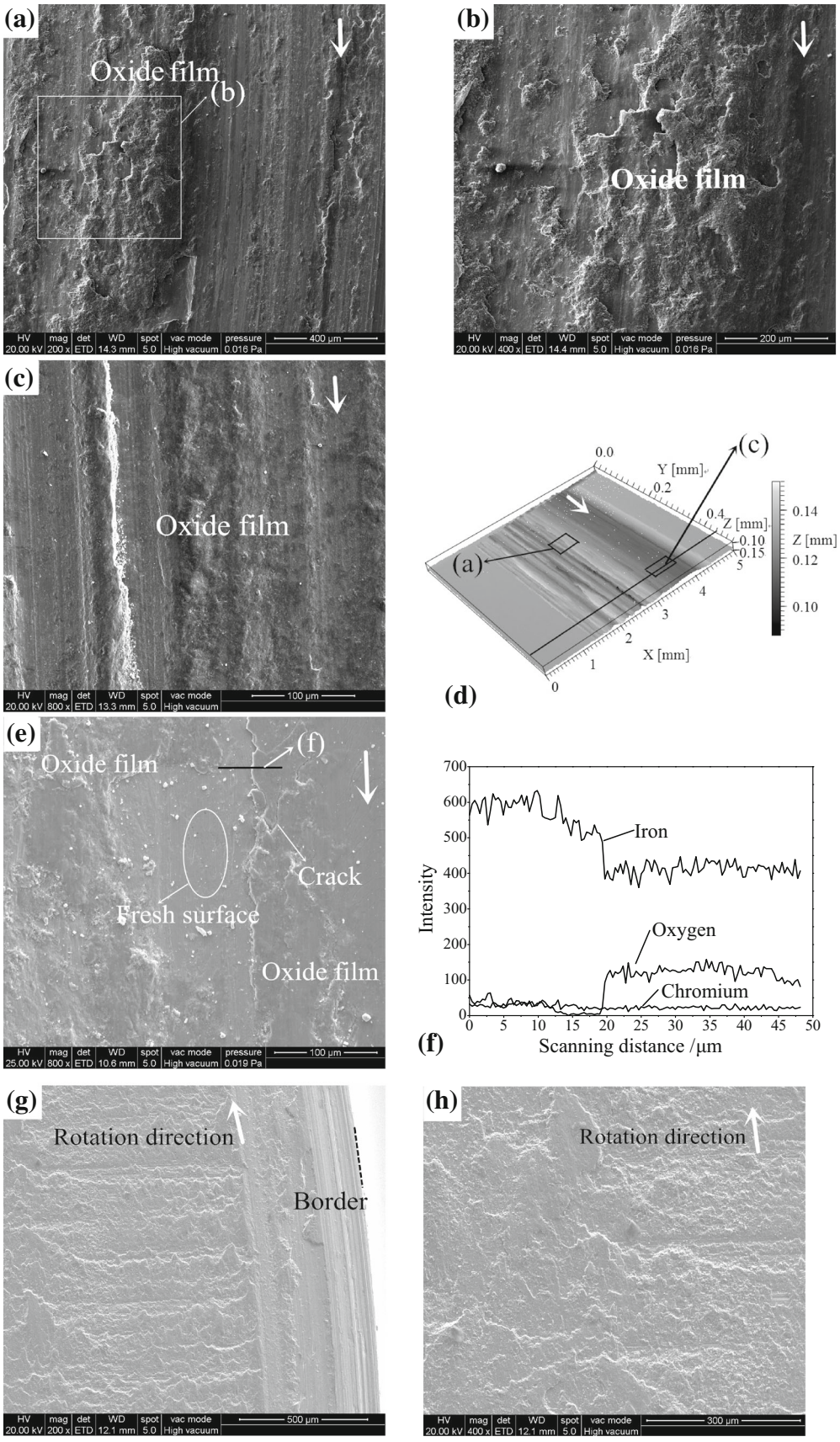

Fig. 7 The microstructure of rubbing surfaces after the test at 400 °C: (a-c) morphologies of worn surfaces of 30CrMnSiA steel, (d) three-dimensional (3D) topography of worn surfaces of 30CrMnSiA steel, (e-f) EDS line scanning analysis of the worn surface, and (g-h) morphologies of worn surfaces of AISI 52100 steel

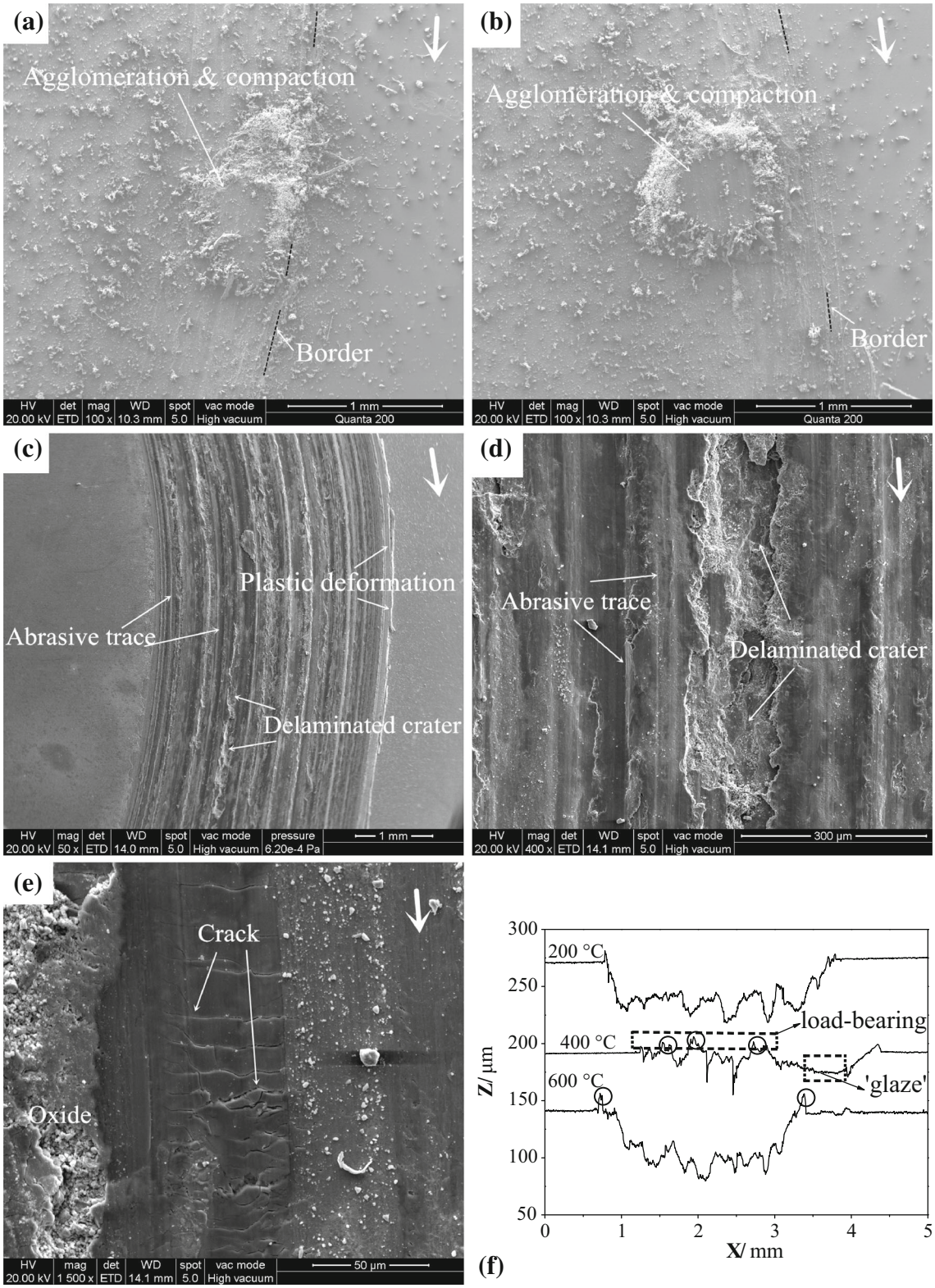

Fig. 8 Morphologies of worn surfaces of 30CrMnSiA steel at 600 °C: (a-b) at the early stages of sliding (200 s) of a specimen (without cleaning), (c-e) after the test for 4200 s, and (f) cross-section profiles of worn surfaces at various temperatures

the wear rate at 600 °C further accelerated compared to 400 °C. From this, it can be said that 400 °C is the critical temperature.

Oxide films were broken by shearing stress and fatigue mechanism under the scratching action of the rubbing surfaces, leading severe delaminated crater on the worn surface. Further, the friction coefficients severely fluctuate in the subsequent stage at 600 °C, due to the damage of the oxide film. Many cracks are also observed on the matrix of worn surfaces (Fig. 8e). It can be inferred that further propagation of cracks may lead to delaminated crater. In conclusion, severe adhesive/

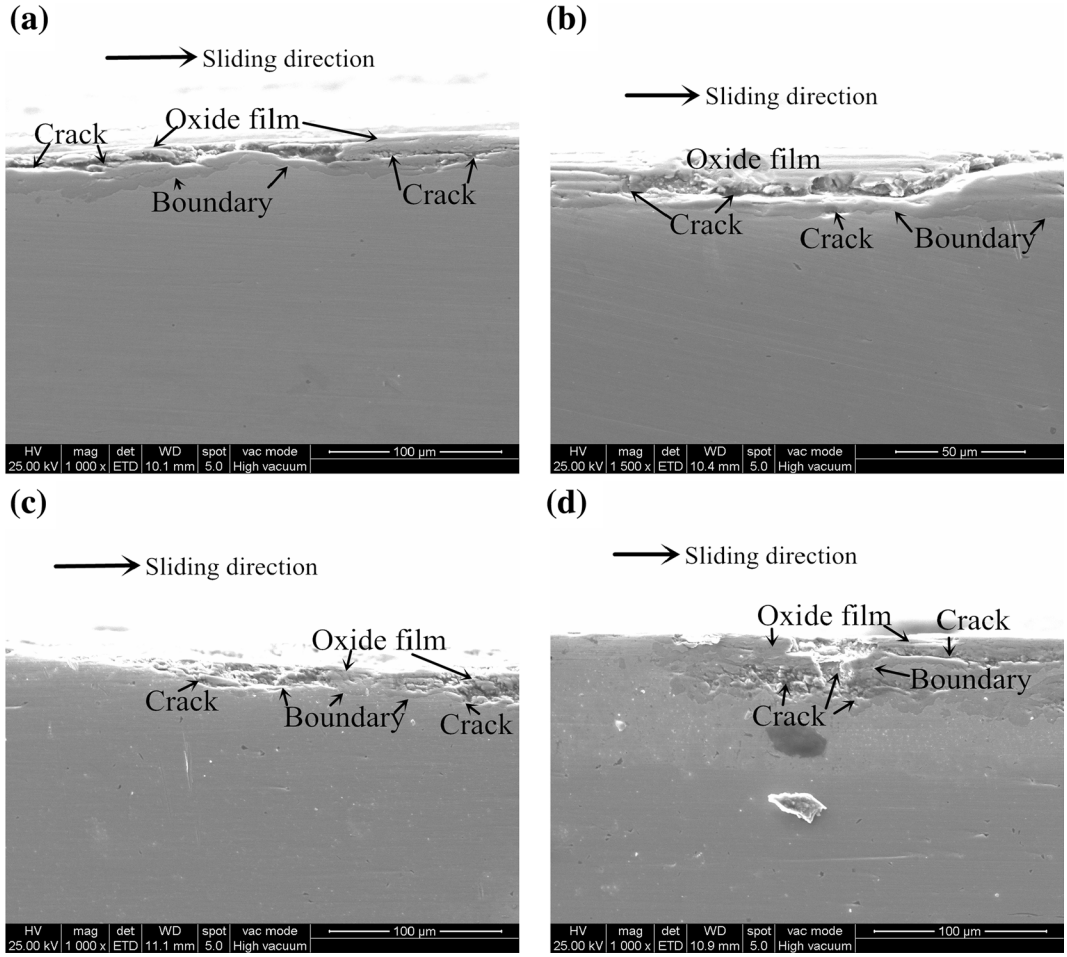

Fig. 9 Delamination patterns and morphology of oxide film on cross-sectional worn surface at 600 °C: (a) inside oxide film, (b) inside oxide film and at the interfaces between the matrix and the oxide film, (c) at the interfaces between the matrix and the oxide film, and (d) at the subsurface of the matrix

delamination wear and severe abrasive wear are found to be the dominant wear mechanisms at high temperature (600 °C) sliding.

Figure 8(f) displays two-dimensional profiles of worn surfaces at various temperatures. The plowed groove at 200 °C is approximately 40 μm deep and 3 mm wide. Numerous oxide 'islands' can be found in the wear track obtained at 400 °C. Those oxides are the wear-protective load-bearing layers covered on the surface. Hence, lowest wear rate was found in the specimen tested at 400 °C. Although the wear track is deeper at 600 °C than that at 200 °C, the relatively lower/smaller width is responsible for its lower wear loss. In addition, plastic deformation of disks causes two 'shoulders' at the edge of wear track.

The cross-sectional micrographs of the worn surfaces tested at 600 °C are illustrated in Fig. 9. Based on the results of Cui and Chen's research on the cast steels at 400 °C, there are three delamination modes of oxide film on worn surface (Ref 11, 27, 28). From Fig. 9, the delamination easily occurs inside oxide film, at the interfaces between the matrix and the oxide film and at the subsurface of the matrix. They further pointed out that the former two patterns occurred during mild oxidation wear at lower wear rate, and the third pattern took place during severe wear at high wear rate.

However, there is a difference in the studied 30CrMnSiA steel. It is found that all three delamination modes of oxide film may occur at 600 °C, even at low wear rate. Figure 9(a) and (b) show that most of the cracks occurred in the oxide film separates the oxide film off the worn surface. In addition, cracks also appear at the boundary between oxide film and matrix (Fig. 9b and c). Moreover, Fig. 9(d) shows the first and third patterns concurrently. Crack may initiate and propagate in matrix under oxide film, finally leads to fracture of part of matrix and oxide film, resulting in an increase in wear rate. During the wear tests, the oxide films were broken by shearing stress and fatigue mechanism with the scratching action of the rubbing surfaces. In summary, all the three delamination modes of oxide film existed in the 30CrMnSiA steel at 600 °C, and it seems to be no explicit correlation between the wear rate and the delamination modes of oxide film.

4. Conclusions

The wear behavior and mechanism of the 30CrMnSiA steel against AISI 52100 steel were systematically evaluated at an ambient temperature range of 100-600 °C, under a normal

pressure of 1.5 MPa at 0.0702 m/s. The conclusions can be drawn as follows:

(1) Temperature has a significant effect on friction and wear behavior of the 30CrMnSiA steel. Both the friction coefficient and wear rate of the steel were lowest at 400 °C.
(2) Various wear mechanisms exist at the high-temperature dry sliding system, but there are dominant mechanisms for each temperature. At lower temperatures (100-300 °C), the hard debris may act as a third body in the rubbing surfaces. Hence, the dominant wear mechanism is found to be abrasive wear. A mild oxidative wear prevailed at 400 °C, due to the formation of a large scale of load-bearing oxide film. At the temperatures of 500 and 600 °C, the substrate was not strong enough to support the oxide film to resist plastic deformation, leading to a mild-to-severe wear transition. Thus, the predominant wear mechanism can be identified as severe abrasive wear and severe adhesive/delamination wear.
(3) The minimal wear rate at 400 °C was caused by the oxide film formation on the worn surface and its mild separation. At 600 °C, the delamination of the oxide film on the worn surface preferentially occurred in the oxide film, at the interfaces between the oxide film and the matrix, and at the subsurface of the matrix.

Acknowledgments

The author would like to thank Professor Hui Guo and Mr. Shi-long Liu of University of Science and Technology Beijing for materials preparation and mechanical properties testing.

Reference

1. S.Y. Chen, C.G. Huang, C.K. Wang, and Z.P. Duan, Mechanical Properties and Constitutive Relationship of 30CrMnSiA Steel Heated at High Rate, *Mater. Sci. Eng. A*, 2008, **483–484**, p 105–108
2. J.S. Zhou, L. Zhen, D.Z. Yang, and H.T. Li, Macro- and Microdamage Behaviors of the 30CrMnSiA Steel Impacted by Hypervelocity Projectiles, *Mater. Sci. Eng. A*, 2000, **282**, p 177–182
3. M.F. Yan, Y.X. Wang, X.T. Chen et al., Laser Quenching of Plasma Nitrided 30CrMnSiA Steel Mater, *Des.*, 2014, **58**, p p154–p160
4. L.N. Tang and M.F. Yan, Influence of Plasma Nitriding on the Microstructure, Wear, and Corrosion Properties of Quenched 30CrMnSiA Steel, *J. Mater. Eng. Perform.*, 2013, **22**, p 2121–2129
5. L.N. Tang and M.F. Yan, Effects of Rare Earths Addition on the Microstructure, Wear and Corrosion Resistances of Plasma Nitrided 30CrMnSiA Steel, *Surf. Coat. Technol.*, 2012, **206**, p 2363–2370
6. J.A. Williams, Wear Modelling: Analytical, Computational and Mapping: A Continuum Mechanics Approach, *Wear*, 1999, **225–229**, p 1–17
7. F.H. Stott, High-Temperature Sliding Wear of Metals, *Tribol. Int.*, 2002, **35**, p 489–495
8. J. Jiang, F.H. Stott, and M.M. Stack, A Generic Model for Dry Sliding Wear of Metals at Elevated Temperatures, *Wear*, 2004, **256**, p 973–985
9. P.J. Blau, Fifty Years of Research on the Wear of Metals, *Tribol. Int.*, 1997, **30**, p 321–331
10. T.F.J. Quinn, Oxidational Wear Modelling Part III. The Effects of Speed and Elevated Temperature, *Wear*, 1998, **216**, p 262–275
11. X.H. Cui, S.Q. Wang, F. Wang, and K.M. Chen, Research on Oxidation Wear Mechanism of the Cast Steels, *Wear*, 2008, **265**, p 468–476
12. S.M. Hsu, M.C. Shen, and A.W. Ruff, Wear Prediction for Metals, *Tribol. Int.*, 1997, **30**, p 377–383
13. Z.M. Liu, Friction and Wear Characteristics of M50 High Speed Steel at Elevated Temperature, *Tribol.*, 1997, **17**, p 38–43
14. X.H. Cui, S.Q. Wang, M.X. Wei, and Z.R. Yang, Effect of Microstructures on Elevated–temperature Wear Resistance of a Hot Working Die Steel, *J. Mater. Eng. Perform.*, 2011, **20**, p 1055–1062
15. V. Abouei, H. Saghafian, and S. Kheirandish, Effect of Microstructure on the Oxidative Wear Behavior of Plain Carbon Steel, *Wear*, 2007, **262**, p 1225–1231
16. X.H. Cui, J. Shan, Z.R. Yang, M.X. Wei, S.Q. Wang, and C. Dong, Alloying Design for High Wear-Resistant Cast Hot-Forging Die Steels, *J. Iron Steel Res. Int.*, 2008, **15**, p 67–72
17. J. Zhang, Y. Peng, H.M. Liu, and Y.F. Liu, Influence of Normal Load, Sliding Speed and Ambient Temperature on Wear Resistance of ZG42CrMo, *J. Iron Steel Res. Int.*, 2012, **19**, p 69–74
18. A.F. Smith, The Sliding Wear of 316 Stainless Steel in Air in the Temperature Range 20–500 °C, *Tribol. Int.*, 1985, **18**, p 35–43
19. F.H. Stott, J. Glascott, and G.C. Wood, The Sliding Wear of Commercial Fe–12%Cr Alloys at High Temperature, *Wear*, 1985, **101**, p 311–324
20. M.X. Wei, S.Q. Wang, L. Wang, X.H. Cui, and K.M. Chen, Effect of Tempering Conditions on Wear Resistance in Various Wear Mechanisms of H13 Steel, *Tribol. Int.*, 2011, **44**, p 898–905
21. G. Straffelini, D. Trabucco, and A. Molinari, Oxidative Wear of Heat-Treated Steels, *Wear*, 2011, **250**, p 485–491
22. H. So, The Mechanism of Oxidational Wear, *Wear*, 1995, **184**, p 161–167
23. I.I. Garbar, Gradation of Oxidational Wear of Metals, *Tribol. Int.*, 2002, **35**, p 749–755
24. Z.Q. Jiang, J.M. Du, and X.L. Feng, Study and Application of Heat Treatment of Multi-element Wear-Resistant Low-Alloy Steel, *J. Iron Steel Res. Int.*, 2006, **13**, p 57–61
25. F.H. Stott, The Role of Oxidational in the Wear of Alloys, *Tribol. Int.*, 1998, **31**, p 61–71
26. J.R. Chen and Y.P. Shi, An Investigation on High Temperature Hardness of Tool Materials, *J Univ. Sci. Technol. Beijing*, 1990, **12**, p 443–450 **(in Chinese)**
27. K.M. Chen, S.Q. Wang, Z.R. Yang, F. Wang, X.H. Cui, and L. Pan, High Temperature Wear and Oxide Film of Steels, *Tribology*, 2008, **28**, p 475–479 **(in Chinese)**
28. X.H. Cui, S.Q. Wang, and Q.C. Jiang, High–Temperature Wear Mechanism of Cast Hot-forging Die Steel 4Cr3Mo2NiV, *Acta Metall. Sin.*, 2005, **41**, p 1116–1120 **(in Chinese)**